Image Cover Sheet

CLASSIFICATION	SYSTEM NUMBER
UNCLASSIFIED	503685

TITLE

TWO-WAY TIME SPREADING AND PATH LOSS IN SHALLOW WATER AT 20-40 kHz

System Number:

Patron Number:

Requester:

Notes:

DSIS Use only:

Deliver to:

Two-Way Time Spreading and Path Loss in Shallow Water at 20–40 kHz

Paul C. Hines, Arthur J. Collier, and James A. Theriault

Abstract— **Two-way time spreading and path-loss measurements were collected in water 100 m deep, off the coast of Nova Scotia. Data were collected at frequencies of 20–22 kHz, 27–29 kHz, and 35–37 kHz using linear FM pulses 0.160 s in duration. The source–receiver was an anchored, high-frequency active sonar, and the target was a free-drifting echo repeater. Sonar and target positions were recorded using a portable tracking range. In the paper, two-way time spreading and path loss measurements are compared with modeled estimates obtained using an enhanced version of the generic sonar model (GSM). The GSM estimates of time spreading due to multipath propagation compare favorably with the experimental data. The model indicates that the path loss for individual eigenrays was extremely sensitive to fluctuations in the sound-speed profile. This led to substantial variation in the model output depending on the choice of profile. In place of the model, an empirical estimate of path loss was computed from the data. We obtained a two-way spreading loss of $2[18.4\log_{10}(R)]$ where R is the range from sonar to target. The data were also used to compute the standard deviation of the received echo intensity at each frequency. The standard deviation was computed two different ways. First it was computed using the peak echo level from each of the pulses at a given frequency. Then, it was computed from the total energy received from each of the pings. At all frequencies, the standard deviation was 1–2 dB lower when computed from the total received energy.**

Index Terms— **High frequency, measurements, propagation loss, shallow water, time spreading.**

I. Introduction

THIS paper presents measurements of two-way time spreading and path loss over the frequency band 20–40 kHz, collected in shallow water off the coast of Nova Scotia. Time spreading measurements provide an indirect measure of the acoustic bandwidth that can be supported by the water channel and path-loss measurements provide a measure of the operational range of a sonar system; both of these data are critical to the design of sonar systems. Although time spreading is an issue of significant current interest, published literature is somewhat scant (c.f. [1]–[3]). Measurements of time spreading are particularly limited. The authors are unaware of any published measurements taken at high frequency in shallow water for the two-way geometry. The experimental measurements were part of a joint Canadian–US–U.K. trial to address this deficiency. In the paper, two-way time spreading and path loss measurements are compared with modeled estimates obtained using an enhanced version of the generic sonar model [4] (GSM). The GSM estimates of time spreading due to multipath propagation compare favorably with the experimental data. However, the model indicates that for the experimental geometry the path loss for individual eigenrays was extremely sensitive to fluctuations in the sound-speed profile. This led to substantial variation in the model output depending on the choice of profile. In place of the model, an empirical estimate of the path loss for three range/frequency combinations was computed from the data. In addition, the data were used to compute the standard deviation of the received echo intensity at each frequency.

Following the introduction, we describe the experiment and the bottom topography of the experimental site. Then the time spreading and path loss data are presented and compared with estimates obtained using GSM. Then, an empirical formula for path loss for the experimental geometry is calculated from the data. Finally, we present some conclusions which resulted from the research.

Manuscript received June 10, 1996; revised January 24, 1997.

The authors are with the Defence Research Establishment Atlantic, Dartmouth, Nova Scotia, Canada, B2Y 3Z7.

Publisher Item Identifier S 0364-9059(97)03399-2.

II. Experimental Equipment and Geometry

Fig. 1 shows a schematic of the geometry for the time spreading experiment. The U.K. echo repeater was deployed to 76-m depth, and the Canadian sonar array, SEAHORSE, was deployed to 42 m. The seabed was nominally flat, with an average water depth over the extent of the experiment of 104 m. The benthic topography is discussed in greater detail in the following section. The experiment was conducted inside the perimeter of a tracking range developed and operated by US personnel. The tracking range allowed accurate positioning of both SEAHORSE and the echo repeater during the experiments. SEAHORSE was decoupled from surface motion using a two-stage decoupling system and anchored to the seabed within the tracking range using a second two-stage decoupling system. The experiment was conducted during a 2-h period throughout which the echo repeater was free drifting. This allowed for measurements at several SEAHORSE-to-target ranges. Fig. 2 shows a plot of the SEAHORSE and the echo repeater GPS tracks measured during the experiment. The start locations of the tracks are as marked. Fig. 3 contains a plot of relative range and bearing from SEAHORSE to the echo repeater over the duration of the experiment. The data in Fig. 3 equate to an average drift speed for the echo repeater of 0.1 m/s.

A. The SEAHORSE System

SEAHORSE is an HF active sonar for collecting environmental acoustic data in the open ocean [5]. The sonar operates

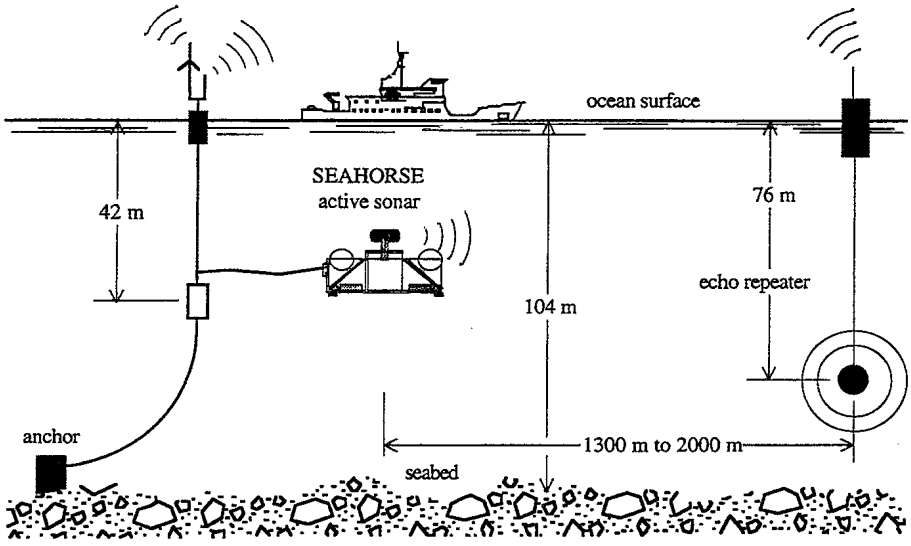

Fig. 1. Schematic of experimental setup. Note that the echo repeater was free drifting during the experiment thereby varying the range from 1300 to 2000 m.

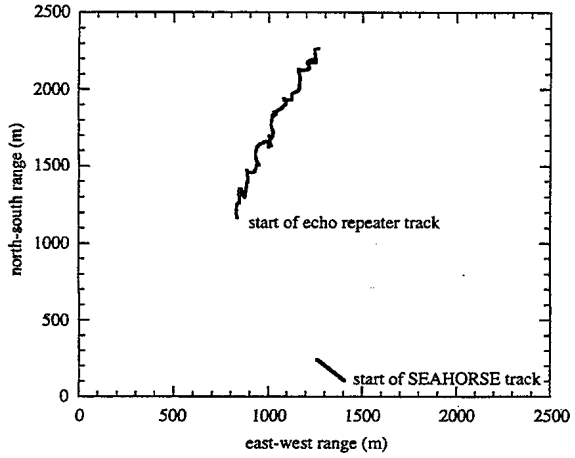

Fig. 2. Tracks of SEAHORSE and echo repeater during the experiment.

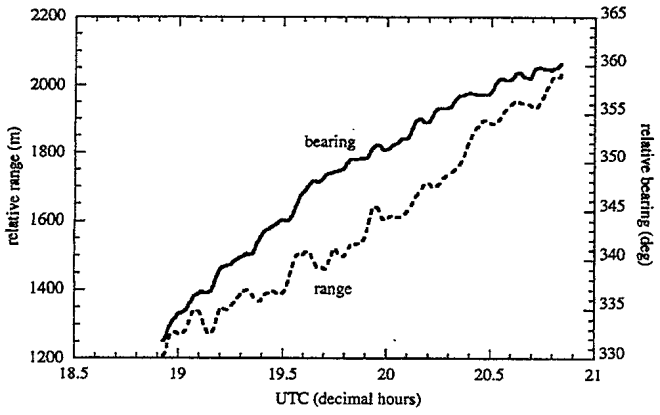

Fig. 3. Relative range and bearing from SEAHORSE to the echo repeater during the experiment.

over the frequency band 20–40 kHz. In conjunction with the acoustic sensors, SEAHORSE is instrumented with a range of nonacoustic sensors to assist in the evaluation of the data. The nonacoustic sensors include depth, tilt, roll, and heading sensors to monitor array position and direction, as well as accelerometers to monitor platform motion. A series of motors contained in the sonar head point the sonar to the required azimuth and tilt. Communication between the research ship and SEAHORSE is handled via two RF links. The first is a one-way UHF data link which is used to transmit the acoustic and nonacoustic data collected by SEAHORSE back to the research ship, CFAV QUEST. The second is a two-way VHF command link which is used to maintain system control (e.g., select pulse type, set amplifier gains, control pointing direction, etc.).

The acoustic transmitter consists of a 48-element array of transducers, shaded such that one obtains an approximately conical beam of 0.1 sr, measured to the −3-dB points. (In cross-section, this equates to a two-sided beamwidth of 20°.) Beam steering is accomplished mechanically. The sonar operates across the frequency band 20–40 kHz with a source strength of 202 ± 3 dB re 1 μPa @1 m. The same 48-element array used for the acoustic transmitter is used as the primary acoustic receiver. As a receiver, the 48-element array of transducers is shaded to obtain an approximately conical beam of 0.1 sr, measured to the −3-dB points. The receive sensitivity is −180 ± 5 dB re 1 μPa^2/Hz across the frequency band 20–40 kHz.

B. The U.K. Echo-Repeater System

A free-drifting echo repeater designed and operated by the U.K.'s Defence Research Agency (DRA) was employed for the target. System control was maintained through a UHF command link operating at approximately 400 MHz. The echo repeater operated at radio-controlled center frequencies of 22, 28, or 37 kHz with a bandwidth at any of these center frequencies of 4 kHz. The target strength was also telemetered and was set to +10 dB during the entire experiment. Both the transmitter and the receiver in the echo-repeater system were omnidirectional. The system contained onboard DAT recorders with a tape storage capacity of 2 h. The system had a battery

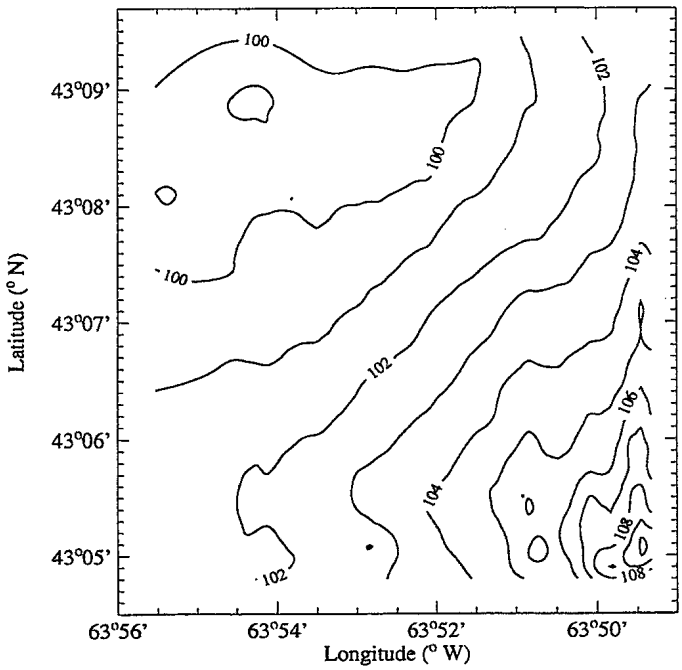

Fig. 4. Contour plot of the water depth (in meters) at the experimental site.

life of 4–6 h continuous and was activated and shut down by command to extend system life.

III. Environmental Description

A. Benthic Topography

The site of the experiment was the eastern flank of the La Have Bank, about 100 nautical miles south of Halifax, Nova Scotia. Fig. 4 shows a contour plot of the bottom for the experimental site. This contour plot was generated from bathymetric data collected with the CFAV QUEST bathymetric system. The bottom was surveyed on two occasions during the trial, once along north–south tracks separated by 500 m between tracks, and on a second occasion with north–south tracks separated by 200 m. A 5-s sampling interval provided samples along the tracks every 15–30 m. These data were combined to produce the set from which the contours were generated. As shown in the plot, the bottom had a gentle slope to the southeast, with the depth increasing from 100 to 110 m over about 10 km. Although there is little small-scale variability in the bathymetry, the bottom at the site is rough. Side-scan sonar and visual records collected at the site during a subsequent trial showed the bottom to be rough to very rough. The bottom is predominately cobble, with the smoothest areas consisting of coarse gravel. In the roughest areas, cobbles were the order of 0.3–3-m diameter. Additional information about the bottom and the experimental geometry is contained in [6].

B. The Water Column

Fig. 5 shows two sound-speed profiles, labeled #21 and #22, taken at the site on the day of the experiment. The third profile, labeled #23 was generated from profile #22 by simply bypassing the narrow minimum occurring between

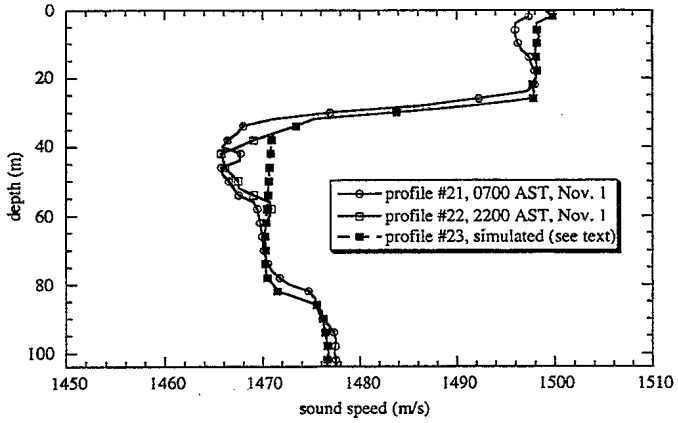

Fig. 5. Two sound-speed profiles of the water column taken on the day of the experiment. The third profile was generated from profile #22 by bypassing the narrow minimum centered at 44 m.

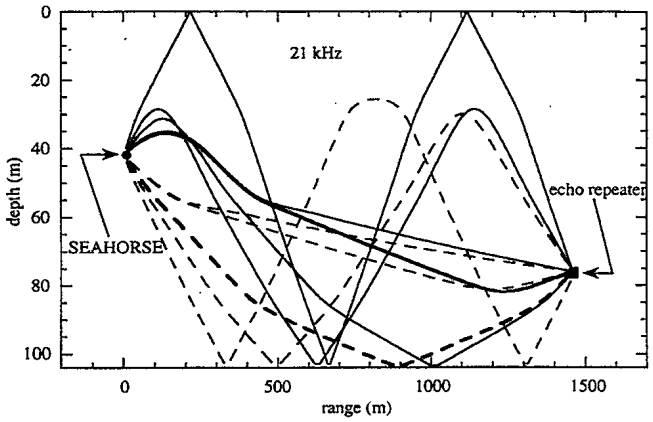

Fig. 6. The 10 dominant eigenrays between the SEAHORSE transmitter and the echo repeater for the 21-kHz geometry. For clarity, rays departing the source toward the surface are solid lines and rays departing the source toward the bottom are dashed. The bold solid line is the most intense ray and the bold dashed line is the first arrival.

35 and 55 m in the latter profile. We shall address the purpose of simulating profile #23 later in the paper. Note the consistent presence of a sound channel in both measured profiles. However, the fine structure of the channel, particularly in the vicinity of the sound-speed minimum, varies due to currents, internal waves, and tidal fluctuations. This variability will be shown to have a significant effect on the modeled path loss but only a marginal effect on the modeled time spreading.

Fig. 6 shows the 10 most intense eigenrays from SEAHORSE to the echo repeater for a source frequency of 21 kHz. Sound-speed profile #22 was used to calculate the eigenrays. The eigenrays exhibited limited surface interaction for the experimental geometry.

IV. Measurements of Time Spreading and Path Loss

The 2-h experiment was conducted in sea state 5 and the wind was reasonably steady from the southeast at 12–15 m/s. ([6] contains a plot of the wind speed for a 24-h period commencing approximately 19 h prior to the experiment.) Three linear FM (LFM) pulse types were used. Each of the 3 LFM pulses were 160 ms in duration with 25% Tukey

shading (12.5% at the start of the pulse and 12.5% at the end of the pulse). The three LFM's had 2-kHz bandwidths spanning frequencies of 20–22 kHz, 27–29 kHz, and 35–37 kHz, respectively. This equates to a temporal resolution (to the −3-dB points) of approximately ±0.17 ms. Throughout the remainder of this paper, each pulse type is referred to by its center frequency: 21, 28, or 36 kHz.

At each frequency, a sequence of 25 LFM pulses was transmitted with a pulse-to-pulse repetition rate of 15 s. For each transmitted pulse, data were recorded for approximately 4 s, starting about 240 ms prior to transmit. We calculated the approximate range from SEAHORSE to the echo repeater acoustically by using the time delay between the start of the transmit pulse and reception of the echo repeater return and a sound speed of 1470 m/s. Synchronization dropouts in the data telemetry link—due to high seas—resulted in a loss of 5–9 LFM pulses in each sequence. Analysis was performed on 16 pulses from each sequence so that the number of time series examined was consistent at all frequencies. During analysis, the pulses were heterodyned down in frequency to the band 500–2500 Hz, low-pass filtered, and subsampled by a factor of eight to reduce data processing and storage requirements. The time series recorded for each pulse was segmented into 4-kiloword samples (50% overlap between samples) and Fourier transformed. The data were matched filtered in the frequency domain using fast convolution.

A. Time Spreading and Path Loss at 21 kHz

Fig. 7 shows a plot of the time spreading returns from two LFM pulses for the 21-kHz run. Each return is normalized to 0 dB at its respective maximum. The two curves were time shifted to align the peak return from the echo repeater for each ping.[1] The open circles and triangles represent the data. The solid line represents the resolution of the matched filter using an exact duplicate of the kernel as the input signal, that is to say, the idealized output of the matched filter. The echo returns typify the ping-to-ping variability in the time spreading data of all 16 of the 21-kHz LFM pulses that were collected. From the figure, one can see that the data are time spread significantly below the −4-dB level.

To indicate the variability of the received echoes, Fig. 8 shows a plot of the target returns from three of the 21-kHz LFM pulses. The plot shows the maximum, the minimum, and the curve nearest to the mean[2] for the two-way path loss as measured relative to the dominant eigenray path (i.e., the peak level of the curve), for the 21-kHz pulses. Using the peak level from each of the 21-kHz LFM pulses, one obtains a standard deviation[3] of 2.3 dB for the two-way path loss.

[1]Throughout the paper, when multiple time spreading data sets are plotted in a single figure, the curves are shifted to align the peak returns. It should be noted that the maximum time shift required to align the peaks for a given run was 25 ms. That is to say, the separation from SEAHORSE to the echo repeater was approximately constant for any frequency run.

[2]Clearly, none of the 16 returns will correpond exactly to the mean level. The curve referred to as the mean target return is actually the curve *nearest in level* to the mean value calculated from the 16 pulses analyzed. The intent here is simply to give the reader a qualitative view of the ping-to-ping variability.

[3]Note that we computed the standard deviation on the logarithmic (decibel) value of the peaks.

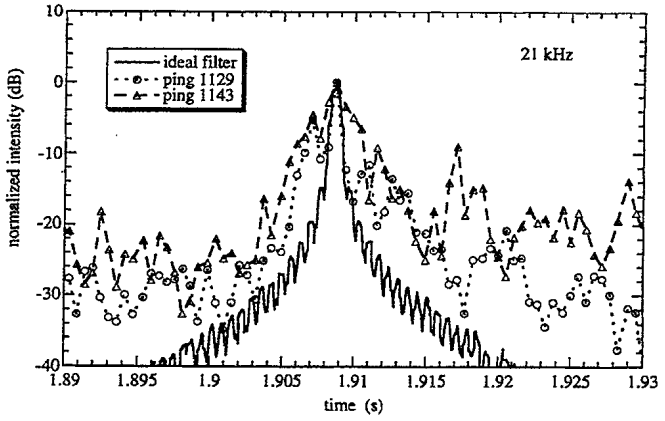

Fig. 7. Target returns from the echo repeater for two "typical" linear FM pings compared to the idealized output of the matched filter (solid line).

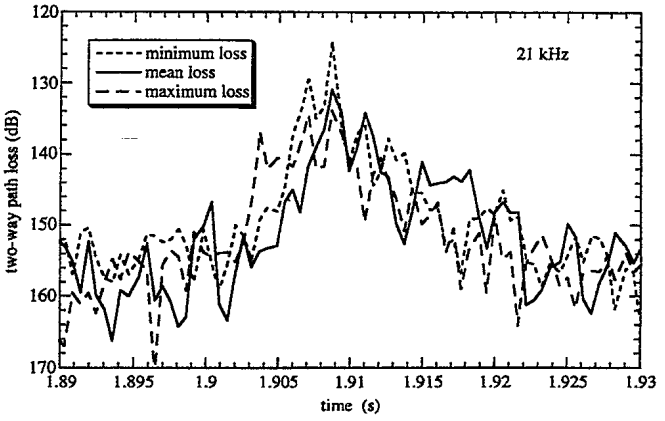

Fig. 8. Data showing two-way path loss and time spreading for the maximum, mean (see footnote 2), and minimum target returns, measured relative to the dominant eigenray path, for each of the 16 pulses at 21 kHz.

Alternatively, one may describe the strength of an echo in terms of the *total energy*[4] returned by the target via all paths. Using this definition, one obtains a standard deviation of 1.7 dB for the two-way loss, for the 16 pulses at 21 kHz. Fig. 9 contains a plot of the data for the curve nearest to the mean for two-way loss as measured relative to the total energy. For comparison, the mean level measured relative to the dominant eigenray path is replotted from Fig. 8. Table I lists the standard deviation using both approaches for the 21-, 28-, and 36-kHz data sets. Plots of the relative intensity of the maximum, the minimum, and the curve nearest to the mean for the 28- and 36-kHz data can be found in [7].

Fig. 10 contains a plot of the averaged target returns for the 21-kHz pulses. The range from SEAHORSE to the echo repeater was approximately 1400 m. Prior to averaging, the matched-filtered data were time shifted to align the peak return from the echo repeater for each ping. The open circles represent the average of all 16 pings. The echo level depicts the two-way path loss and the width of the echo is a measure of time spread. The solid line in the figure shows the resolution of

[4]For the purposes of computation, we approximate the total energy of a curve to include the area under the curve down to −20 dB below its peak level.

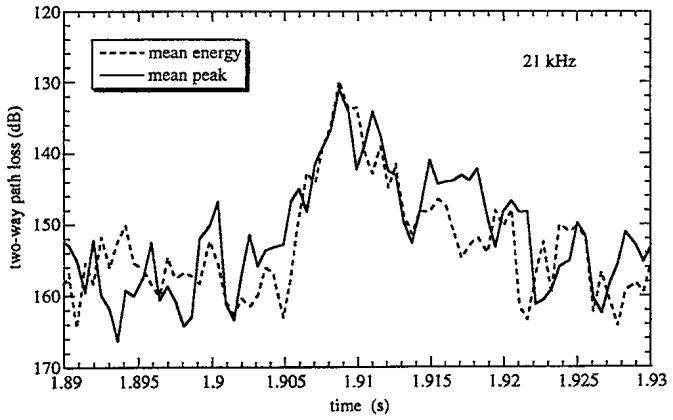

Fig. 9. Data showing two-way path loss and time spreading for the mean target return (see footnote 2), measured relative to the total energy returned by the target via all paths, for each of the 16 pulses at 21 kHz. For comparison, the mean level measured relative to the dominant eigenray path is replotted from Fig. 8.

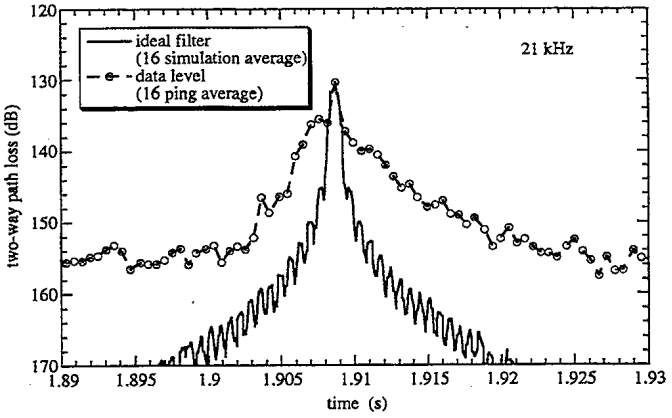

Fig. 10. Averaged data for 16 pings (circles), normalized to 0 dB at its maximum, compared to the idealized output of the matched filter (solid line), for the 21-kHz run.

TABLE I
STANDARD DEVIATION (σ) OF THE TWO-WAY PATH LOSS FOR LINEAR FM (LFM) PULSES IN INDIVIDUAL FREQUENCY BANDS

Frequency (kHz)	σ (dB) using peak level	σ (dB) using total energy
21	2.3	1.7
28	6.5	4.7
36	4.5	2.2

The standard deviations are computed for echo strength expressed as peak amplitude and total received energy.

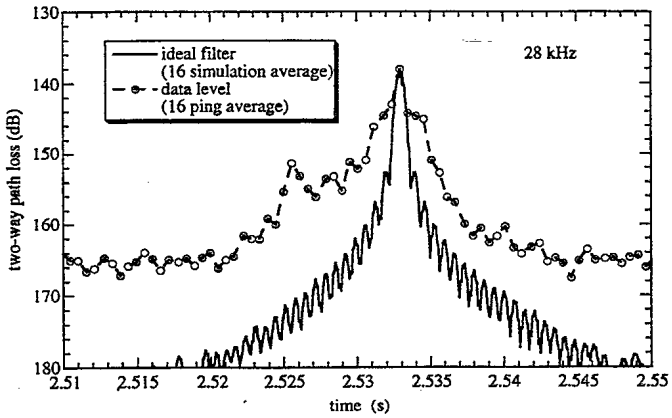

Fig. 11. Averaged data for 16 pings (points), normalized to 0 dB at its maximum, compared to the idealized output of the matched filter (solid line), for the 28-kHz run.

the matched filter. This curve was generated by using an exact duplicate of the kernel as the input signal. To remain consistent with the data, the solid line was obtained by averaging the matched-filter output of 16 realizations of the input signal, each input signal having a slightly different time delay. In this way, any smearing of the data resulting from misalignment of the FFT window[5] and the received echoes will be included in the ideal matched-filter curve. Note that the amplitude of the filter has been normalized to coincide with the maximum of the data. The averaged data substantiates the observation made earlier in reference to time spreading of the individual pings in Fig. 7, i.e., little or no time spreading occurs in the region of the peak, down to about −4 dB but below −4 dB the time spreading increases substantially. Furthermore, the averaged data indicate that the spreading is extremely asymmetric about the maximum. The data are reverberation-limited for losses greater than about 156 dB.

B. Time Spreading and Path Loss at 28 kHz

Fig. 11 shows the averaged target returns for the 28-kHz pulses. The range from SEAHORSE to the echo repeater was approximately 1860 m. Prior to averaging, the matched-filtered data were time shifted to align the peak return from the echo repeater for each ping. The open circles represent the average path loss of all 16 pings. The solid line shown in the figure represents the output of the idealized matched filter using an exact duplicate of the kernel as the input signal. To remain consistent with the data, the solid line was obtained by averaging the matched-filter output of 16 realizations of the input signal, each input signal having a slightly different time delay. Note that the amplitude of the filter has been normalized to coincide with the maximum of the data. As was the case for 21 kHz, the 28-kHz data are time-spread significantly below about the −4-dB level. However, in contrast to the 21-kHz case, the 28-kHz data are not as asymmetric about the maximum and the most significant time spreading occurs before, not after, the dominant eigenray arrival. Note that ambient noise—not reverberation—is the limiting noise source at 28 kHz and masks any returns having a path loss greater than about 166 dB.

C. Time Spreading and Path Loss at 36 kHz

Fig. 12 shows the averaged target returns for the 36-kHz run. The figure also includes the idealized matched-filter output, computed as described previously for Figs. 10 and 11. The range from SEAHORSE to the echo repeater was approximately 1950 m. Prior to averaging, the matched-filtered

[5] Using a Tukey-shaded transmit pulse and 50% overlap in the fast convolution routine ensures that the smearing loss is less than 1 dB.

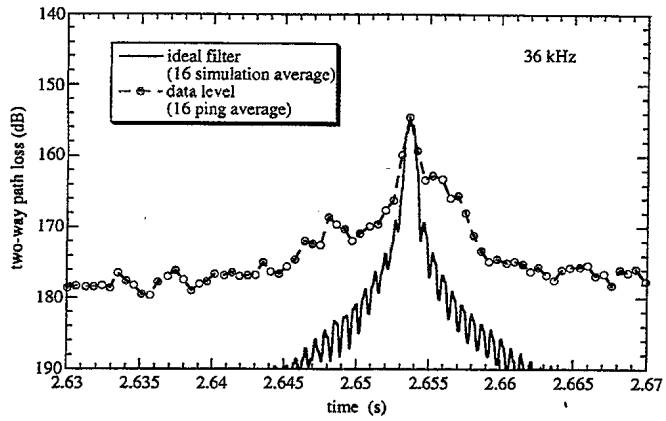

Fig. 12. Averaged data for 16 pings (points), normalized to 0 dB at its maximum, compared to the idealized output of the matched filter (solid line), for the 36-kHz run.

data were time shifted to align the peak return from the echo repeater for each ping. The open circles represent the average path loss of all 16 pings. The solid line shown in the figure represents the output of the idealized matched filter. Note that the amplitude of the filter has been normalized to coincide with the maximum of the data. The data in Fig. 12 indicate that at 36 kHz, the time spread is only significant below the −8-dB level. Ambient noise is the limiting noise source at 36 kHz and masks any returns having a path loss greater than about 178 dB.

In the following section, we compare the time spreading data with results modeled using an enhanced version of the GSM to gain some insight into the cause of the measured time spreading.

V. Comparison of Time-Spreading Data to GSM

Time spreading and path loss for the experimental geometry were modeled using an enhanced version of GSM. We compare the modeled time spreading to the data in strictly phenomenological terms. That is to say, can one understand the spread of the data in light of the eigenray arrivals computed by GSM? In contrast, we examine path loss in more quantitative terms—on the basis of the measured (and modeled) intensity of the main peak(s). Thus, when examining the time spreading issue, it is more instructive to compare the agreement between the model and data if both are normalized to a common reference level (thereby avoiding any distraction introduced by differences in amplitude). Therefore, in this section, we shall compare the (normalized) modeled time spreading with the (normalized) data and defer discussion of the modeled path loss until the following section.

Measured inputs to GSM included the transmit and receive beam patterns for SEAHORSE, sound-speed profile[6] #22 from Fig. 5, a wind speed of 25 knots, and an omnidirectional target strength of 10 dB for the echo repeater. We assumed a pulse length of 0.67 ms to obtain a temporal resolution equivalent to that of the LFM pulses. (This equivalence assumes that no decorrelation of the LFM pulses occurred.)

[6]Profile #22 (recall Fig. 5) was used because it was taken closest to the time of the experiment.

TABLE II
Bottom Reflection Coefficient Table Employed for GSM Calculations

Grazing angle (degrees)	Bottom reflection coefficient (dB)
0.0	-0.00
2.0	-2.00
4.0	-4.00
6.0	-6.00
8.0	-8.00
10.0	-8.00
20.0	-8.00
90.0	-8.00

The bottom backscattering strength was estimated using a Lambert's law dependence with a coefficient of −27 dB. Reverberation measurements made at the site [6] support this backscatter dependence. However, as noted previously, reverberation was only the limiting noise source at 21 kHz. The bottom reflection coefficients proved the most difficult GSM inputs to estimate. This resulted from the lack of quantitative bottom information currently available for the site[7]. Table II contains the bottom reflection coefficients employed. These numbers represent "reasonable" values and provide an acceptable fit to the data. Note that the bottom reflection coefficient at grazing angles greater than 8° does not affect the results for this geometry.

GSM was enhanced to compute the two-way time spreading. To do this, we first calculated the one-way eigenrays from SEAHORSE to the echo repeater. The source level and arrival time of each of these eigenrays were then used as sources for the echo repeater and, using these time-dependent sources, the return-path arrivals were computed. The contributions from each path combination were summed incoherently. The GSM-modeled reverberation level was added to the time-dependent echo, to obtain the estimate of total received intensity. GSM's signal excess subroutine CMPAX1 was modified to perform these calculations.

As indicated in Fig. 3, the echo repeater opened from SEAHORSE at a rate of approximately 0.1 m/s during the experiment. This drift rate resulted in a change of range of 30–80 m (1%–3% of the total range) during the time taken to transmit the ping sequence for a given frequency. To include the range-averaging effects in the modeled results, 16 GSM estimates were taken at each frequency to correspond to the 16 experimental pings. For simplicity, we calculated the start and stop range for each frequency sequence from the measured time delays and assumed a constant drift rate and a sound speed of 1470 m/s to estimate the intermediate ranges. The measured increase in range during both the 21- and 28-kHz experiments was 30 m and thus the model estimates were computed at 2-m range increments. The measured increase in range during the 36-kHz experiment was 75 m and thus the model estimates were computed every 5 m. If the modeled returns are averaged, as was done with the experimental data,

[7]Since the time of writing, side scan sonar data have been obtained at the site. Once analyzed, these data will provide a more quantitative description of the bottom.

the peaks shown in the single modeled returns will be slightly smeared. By way of example, [7, Fig. 18] shows the sensitivity of the GSM output to small variations in range for the 28-kHz geometry.

Recall from Table I that the standard deviation computed from the peak amplitudes of the 16 pings varied from 2.3 to 6.5 dB. These values are considerably greater than the standard deviation of the 16 model estimates, which was approximately 1 dB at all frequencies. That is to say, the ping-to-ping intensity fluctuations measured experimentally are largely unaccounted for in GSM. Therefore, when computing the average time spread from the data, each ping was normalized to 0 dB at its maximum, prior to averaging. This meant that each ping had an equal weighting and ensured that no single ping dominated the average, thereby providing a more effective comparison with GSM[8]. In the subsequent discussion, we shall refer to the data normalized to 0 dB at its maximum *prior to* averaging as the weighted data, and the data normalized to 0 dB at its maximum *after* averaging as the unweighted data. Note that the data shown previously in Figs. 10–12 were unweighted.

A. GSM/Data Time-Spreading Comparisons at 21 kHz

Fig. 13 contains a comparison of the average of the modeled echoes for the 21-kHz sequence with both the weighted and unweighted average for the 21-kHz data, for a nominal SEAHORSE to echo repeater separation of 1400 m. Squares represent the weighted average data, open circles represent the unweighted average data, and the solid line represents the model estimate. The GSM eigenray output (not shown) indicates that the direct path is neither the dominant arrival nor the earliest arrival. It is rather laborious (and not particularly instructive) to associate each modeled peak with its respective eigenray due to the combined effect of the two-way propagation employed in the model and the averaging of the model output. However, it is worth mentioning by way of example that the dominant eigenray for the 21-kHz data is the ray that departs SEAHORSE upward (i.e., toward the surface), then refracts downward and finally refracts upward before arriving at the echo repeater. This eigenray is the emboldened solid line in Fig. 6. For comparison, the first arrival is the single bottom reflection path shown as the emboldened dashed line in Fig. 6.

Clearly, there is less than perfect agreement between the model and the experimental data. The model does however, explain the dominant feature in the data—the asymmetry of the data about its peak amplitude. This feature is consistent with the distribution of peaks predicted by GSM. That is to say, GSM predicts far fewer arrivals prior to the dominant peak than after. Although secondary peaks are not visible in the data, the relative amplitudes of the peaks in the model are consistent with the general decay in amplitude of the data after the arrival of the dominant peak. Furthermore, recall from Fig. 6 that the dominant peak has no surface or bottom interaction, whereas the peak at 1.898 s as well as the peaks located at 1.914 s and later both have bottom and/or

[8]A consequence of the small standard deviation in the model (≈1 dB) is that the weighted and unweighted averages obtained from the model are very similar. In the data-model comparison that follows, the authors have used the unweighted averages obtained from the model.

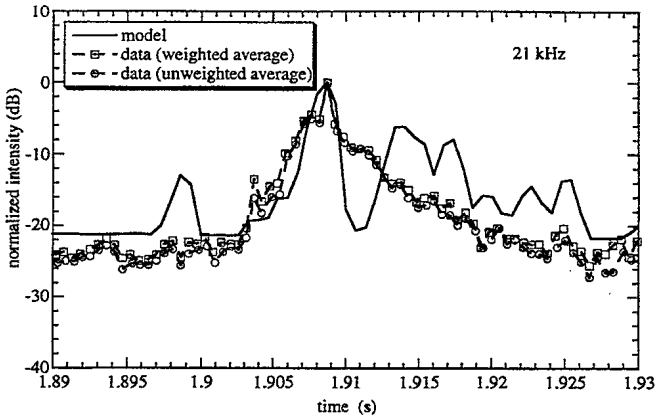

Fig. 13. Averaged data for the 16 pings at 21 kHz, compared to the averaged output of the GSM for 16 ranges at 2-m increments (solid line). Both a weighted data average (squares), computed by normalizing to 0 dB prior to averaging, and an unweighted data average (circles), computed by normalizing after averaging are shown (refer to text).

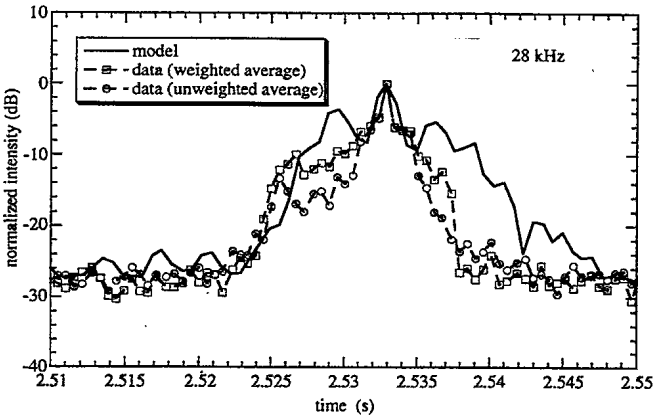

Fig. 14. Averaged data for the 16 pings at 28 kHz, compared to the averaged output of the GSM for 16 ranges at 2-m increments (solid line). Both a weighted data average (squares), computed by normalizing to 0 dB prior to averaging, and an unweighted data average (circles), computed by normalizing after averaging are shown (refer to text).

surface interactions. This provides phenomenological evidence at least that one might alter the bottom reflection coefficients in Table II to reduce these secondary peaks without reducing the dominant one, thereby improving the fit between GSM and the data. However, without quantitative information on the bottom parameters, the exercise would not be particularly instructive. More importantly, any improvement in the fit is unlikely to account for the discrepancy between the data and the model in the immediate vicinity of the dominant peak. That is to say, there is significant time spreading of the dominant data peak beyond that attributable to multipath propagation. It seems unlikely that the spreading in the data results from ocean surface motion since the model predicts no surface interaction for the dominant path. Nor is platform motion likely to be responsible since both SEAHORSE and the echo repeater were nearly motionless.

B. GSM/Data Time-Spreading Comparisons at 28 kHz

Fig. 14 contains a comparison of the average of the modeled echoes at 28 kHz with both the weighted and unweighted

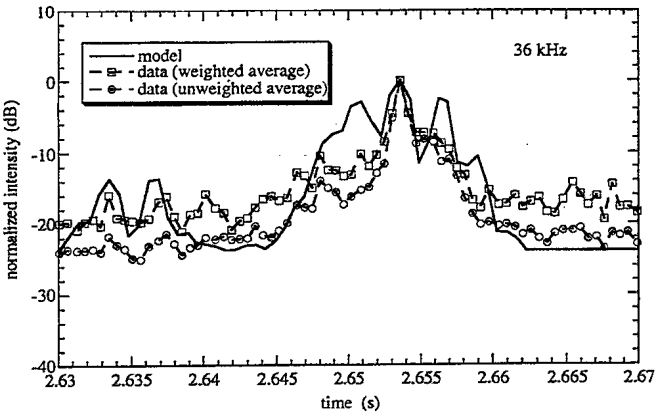

Fig. 15. Averaged data for the 16 pings at 36 kHz, compared to the averaged output of the GSM for 16 ranges at 5-m increments (solid line). Both a weighted data average (squares), computed by normalizing to 0 dB prior to averaging, and an unweighted data average (circles), computed by normalizing after averaging are shown (refer to text).

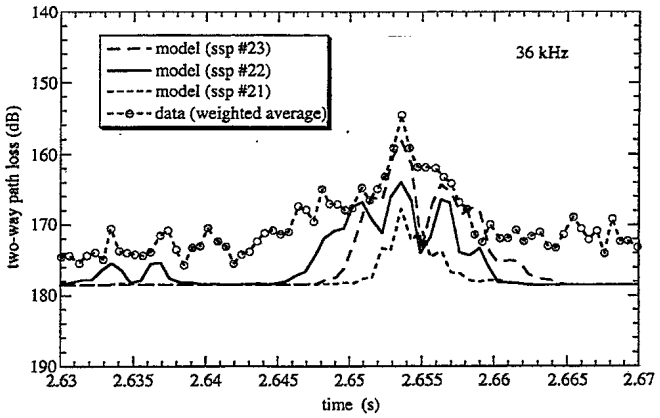

Fig. 16. Sensitivity of the modeled path loss to variations in the sound-speed profile for the 36-kHz data.

average for the 28-kHz data. The nominal separation from SEAHORSE to the echo repeater during this ping sequence was 1860 m. Squares represent the weighted average of the data, open circles represent the unweighted average of the data, and a solid line represents the model estimate. As in the 21-kHz case, the structure of the data is reasonably well modeled by GSM. Both the data and the model are significantly more symmetric about the maximum than at 21 kHz. The 28-kHz data are time-spread relative to the ideal matched filter (recall Fig. 11). However, the model results suggests that multipath propagation should have resulted in even greater time spreading than that exhibited by the data. However, this discrepancy between GSM and the data may result from inaccuracies in the bottom loss table, as discussed previously. It should be noted that ambient noise, not reverberation, provides the background level at 28 kHz.

C. GSM/Data Time-Spreading Comparisons at 36 kHz

Fig. 15 contains a comparison of the average of the modeled echoes at 36 kHz with both the weighted and unweighted data, for a nominal SEAHORSE to echo repeater separation of 1950 m. Squares represent the weighted average of the data, open circles represent the unweighted average of the data, and a solid line represents the model estimate. Note that the three peaks appearing in the weighted data from 2.633–2.641 s were buried in the unweighted average. Once again, the structure of the data is reasonably well modeled by GSM. As for the 28-kHz case, the model predicts more extensive time spreading than that exhibited by the data.

VI. Comparison of Measured Path Loss to Model Estimates

As stated in the introduction, the path loss was sensitive to fluctuations in the sound-speed profile for the experimental geometry. This leads to substantial differences between model estimates and the data. Fig. 16 depicts the modeled sensitivity for the 36-kHz data. The figure contains path loss estimates computed from GSM for the two measured sound-speed profiles, as well as an estimate computed using the simulated sound-speed profile shown in Fig. 5. The figure also contains the averaged path loss measured during the experiment. The seemingly inconsequential differences from profile #21 to #22 result in a decrease in the path loss estimate of 3 dB at the peak. Even profile #22 results in a modeled path loss some 10 dB greater than that measured. However, eliminating the narrow minimum in profile #22 as was done to generate profile #23, reduced the path loss estimate by another 7 dB. Clearly, for the experimental geometry, the path loss estimated by the model is extremely sensitive to the sound-speed profile used.

TABLE III
Path Loss Measured at the Three Frequencies

freq (kHz)	range (m)	two-way path loss (dB)	absorption (α) (dB/m)	spreading loss (dB)	spreading loss coefficient (A)
21	1402.9	130.44	$3.72(10^{-3})$	120.00	19.07
28	1861.7	138.05	$5.99(10^{-3})$	115.75	17.70
36	1950.4	154.62	$8.68(10^{-3})$	120.76	18.35

The values of absorption were interpolated from [8, Table IV].

In light of the poor match between the model and the measurements, we instead computed an empirical estimate of the path loss from the data. We begin by writing the two-way path loss in the form

$$\mathrm{PL} = 2\alpha R + 2A \cdot \mathrm{Log}_{10}(R/R_0) \qquad (1)$$

where R is the one-way range in meters from source–receiver to the target, (R is referenced to a source level measured at $R_0 = 1$ m), α is the absorption in dB/m, A will be referred to as the spreading loss coefficient, and the 2 in both right-hand-side terms accounts for the two-way path length. The first term in (1) is the absorption loss and the second term is the spreading loss. For spherical spreading in an isovelocity medium $A = 20$ and for cylindrical spreading in an isovelocity medium $A = 10$. Table III contains values of PL and R measured for the three frequencies. Estimates of α were interpolated from [8, Table IV]. From Table III, one obtains an average spreading loss coefficient of $A = 18.4 \pm 0.7$.

VII. Discussion

The energy calculation of the standard deviation indicates that there is significant ping-to-ping variability in the energy. This likely occurs since ping-to-ping fluctuations redistribute the energy into paths which do not intercept the target or since more energy is scattered incoherently through surface and/or bottom interactions from one ping than from another. No attempt was made to model this because GSM models path loss as a deterministic process. That is to say, the GSM results do not have any statistical fluctuations built into the eigenray calculation.

At all three frequencies, the standard deviation was lower when computed using the total energy than when computed using the peak value (recall Table I). This is because the peak value calculation results from a single eigenray and small changes in range affect the amount of energy in the dominant eigenray. In contrast, the energy calculation is less sensitive to these fluctuations since a significant portion of the energy stripped from one eigenray will reach the receiver via slightly different path(s). Note that the *difference* in the value of the standard deviation obtained from the energy calculation and the peak level calculation is in good agreement with the standard deviation of $\approx$1 dB obtained from the model, which was cited in the previous section.

Although GSM provides a qualitative explanation of the time spreading, there are definite discrepancies between the model and the data. For example, the 21-kHz data in Fig. 13 exhibit significantly more time spreading immediately after the arrival of the dominant peak than estimated by the model. Also, in Figs. 14 and 15, the several well-defined peaks around the maximum obtained from GSM are not all observable in the data. This is not surprising since GSM is a CW model and the pulses used during the experiment were 2 kHz wide. This makes it difficult to model the time spreading in detail. It is possible that the agreement would improve if one had more accurate inputs into GSM for the bottom loss, the backscattering strength, and the SEAHORSE-to-target separation for each ping. However, the range-independent nature of GSM will clearly limit one's ability to match the fine structure of the data.

The disagreement between path loss data and the model results from the sensitivity of acoustic propagation to the sound speed profile for the experimental geometry. With the source–receiver located at the minimum of the sound-speed profile, and the target located at the lower edge of the sound channel, it is not surprising that the choice of profile significantly impacts the modeled path loss. What is perhaps surprising is the magnitude of the effect: employing the three profiles contained in Fig. 5 in the model resulted in path loss estimates differing by as much as 10 dB. The sensitivity of the model to the profile is noteworthy since in coastal environments the assumption of a range-independent sound-speed profile is somewhat unrealistic to begin with. Finally, it is worth considering the effect of nonspherical spreading on the path loss. For example, given a sonar-target separation of 2000 m, spherical spreading results in a two-way spreading loss of 132 dB. Alternatively, a spreading loss coefficient of 18.4 reduces that loss to 122 dB, i.e., a reduction of 10 dB in the path loss. Clearly, even small departures of A from its spherical spreading value can result in significant changes in propagation.

VIII. Summary and Conclusion

Time spreading and path loss measurements were collected in a water channel 100 m deep, off the coast of Nova Scotia. Data were collected at center frequencies of 21, 28, and 36 kHz using linear FM pulses 0.16 s in duration with a 2-kHz bandwidth. An anchored high-frequency active sonar was employed for the source–receiver, and a free-drifting echo repeater was employed for the target. Source–receiver and target position were recorded using a portable target range. At each frequency, time-spreading measurements obtained from averaging the returns from 16 pings were compared with estimates obtained from an enhanced version of the GSM. The estimates were extremely sensitive to fluctuations in the sound-speed profile for the experimental geometry. This led to substantial differences between the model and the data. In place of the model, we derived an empirical path loss formula from the data. Additionally, the standard deviation of the received echo intensity from the 16 pings was computed.

The standard deviation of the received echo intensity was computed two ways. First it was computed from the peak echo level from each of the 16 pulses at a given frequency. Then, it was computed from the total energy received from each of the 16 pings. At all three frequencies, the standard deviation was lower by 1–2 dB when computed from the total received energy. This is likely because the maximum value results from a single eigenray and the energy in the dominant eigenray closely depends on small changes in range, etc. In contrast, the energy calculation is less sensitive to these fluctuations since a significant portion of the energy will still reach the receiver via slightly different paths.

At each frequency, the average time spreading was normalized to 0 dB with respect to the maximum. These data were compared to the output of an ideal matched filter with the following results. At 21 and 28 kHz, little or no time spreading occurred in the region of the peak, down to about the −4-dB points. Below −4 dB, however, the time spreading increases substantially. At 36 kHz, the time spreading only becomes significant below the −8-dB points.

GSM provides an acceptable qualitative explanation of the time spreading, particularly in describing the overall width and shape of the main returns. At 21 kHz, the time-spreading data were extremely asymmetric about the maximum in the data, whereas at 28 and 36 kHz the data were somewhat more symmetric. The GSM results indicate that the degree of symmetry resulted from the arrival time and amplitude of the various eigenrays. There were some definite discrepancies between the model and the data. At 21 kHz, the data exhibited significantly more time spreading in the vicinity of the maximum than estimated by the model. At 28 and 36 kHz, the GSM output exhibited several clear peaks which were not well defined in the data. It is reasonable to expect the agreement to improve if one had more accurate inputs into GSM for the bottom

loss, the backscattering strength, and the SEAHORSE-to-target separation for each ping. However, the range-independence of GSM and its CW formulation will clearly limit one's ability to match the fine structure of the data for this experiment.

The disagreement between the model and the path-loss measurements results from the sensitivity of both model and data to the sound-speed profile for the experimental geometry. This clearly demonstrates the importance of good environmental measurements in shallow water. This is an important issue in coastal environments since tidal flow, currents, and internal waves will lead to frequent temporal and spatial fluctuations in the sound speed. Finally, we used the data to calculate an empirical formula for spreading loss for the experiment. We obtained a value of 18.4 ± 0.7 for the spreading coefficient which leads to significantly lower path loss than one would obtain via spherical spreading.

ACKNOWLEDGMENT

The authors wish to acknowledge the contributions of the experimental team from DREA, R. Lee Culver and the experimental team from The Applied Research Laboratory, The Pennsylvania State University, and The Applied Research Laboratory, Keyport, WA, D. Jepsen and the experimental team from NUWC-Keyport, and M. Bishop and the experimental team from The Defence Research Agency, U.K. The authors also wish to acknowledge NUWC for release of GSM to Defence Research Establishment Atlantic.

REFERENCES

[1] M. H. Brill, X. Zabel, and S. L. Adams, "Time spread of acoustic signals reflecting from a fixed rough boundary," *J. Acoust. Soc. Amer.*, vol. 75, pp. 1062–1070, 1984.

[2] S. L. Adams and J. W. Doubek, "Frequency coherence and time coherence in random multipath channels," *J. Acoust. Soc. Amer.*, vol. 62, pp. 286–294, 1977.

[3] P. H. Dahl and A. Al-Kurd, "Time spread and frequency coherence in acoustic forward scattering from the sea surface," Applied Physics Laboratory, University of Seattle, WA, APL-UW TR 9405, 1994.

[4] H. Weinberg, "The generic sonar model," Naval Underwater Systems Center, New London, CT, Tech. Document 5971D, 1985.

[5] P. C. Hines, J. S. Hutton, and A. J. Collier, "A free floating, steerable, HF sonar for environmental measurements," in *IEEE Oceans'93 Conf. Proc.*, 1993, vol. 2, pp. 65–70.

[6] P. C. Hines and D. D. Ellis, "High-frequency reverberation in shallow water," *IEEE J. Oceanic Eng.*, this issue, pp. XX–XX.

[7] P. C. Hines, A. J. Collier, and J. S. Hutton, "Time spreading at high frequency in a shallow water channel," *DREA/TM/96/209*, 1996.

[8] R. E. Francois and G. R. Garrison, "Sound absorption based on ocean measurements. Part II: Boric acid contribution and equation for total absorption," *J. Acoust. Soc. Amer.*, vol. 72, pp. 1879–1890, 1982.

Paul C. Hines was born in Glace Bay, Nova Scotia, Canada, in 1958. He received the B.Sc. (Hon.) degree in engineering physics from Dalhousie University, Halifax, Canada, in 1981 and the Ph.D. degree in physics from the University of Bath, U.K., in 1989.

From 1981 to 1985, he was a Scientist in the Sonar Projects group at Defence Research Establishment Atlantic (DREA), working in the field of towed array self-noise. Upon returning from the University of Bath in 1989, he joined the Acoustic Countermeasures group at DREA to work on scattering and time spreading. Presently, he is Leader of the Airborne Sensors group at DREA. His present research interests include acoustic scattering and frequency and time spreading.

Dr. Hines is a member of the Acoustical Society of America.

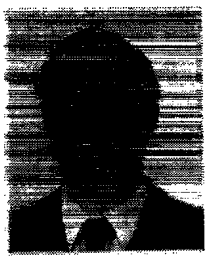

Arthur J. Collier was born in Victoria Britich Columbia, Canada, on December 31, 1944. He received the B.Sc. degree in physics from the University of Alberta, Edmonton Alberta in 1966 and the M.Sc. degree in physics (nuclear spectroscopy) from the University of Regina, Regina Saskatchewan, in 1969.

At this time, he joined Defence Research Establishment Atlantic (DREA) where he has been employed since, with the exception of a two-year exchange at the Naval Research Laboratory in Washington, DC, from 1982 to 1984. His major focus in research has been on the acoustic environment, naval sonars and sonobuoys, sonar signal processing, and torpedo defence. Over the 1990–1995 tenure of the Acoustic Countermeasures group at DREA, he was the group leader, and his current interest remains focused in this area.

Mr. Collier is a member of the Acoustical Society of America and the Canadian Acoustical Association.

James A. Theriault was born in Halifax, Nova Scotia, Canada, in 1961. He receiving the B.Sc. (Hon.) and M.Sc. degrees in mathematics from Dalhousie University, Halifax, in 1984 and 1985, respectively.

He joined Defence Research Establishment Atlantic (DREA) as a Scientist in the Mathematical Analysis group working on sonar system studies and target motion analysis. Currently, his research interests include modeling active-sonar-system techniques with an emphasis on three-dimensional effects, frequency, and time spreading.

Mr. Theriault is a member of the Acoustical Society of America.

#523685